To be published in *J. Alloys & Compounds*

High temperature transformations of the $Au_7Cu_5Al_4$ shape-memory alloy

Michael B. Cortie[a], Catherine S. Kealley[a], Vijay Bhatia[a], Gordon J. Thorogood[b], Margaret M. Elcombe[c], and Maxim Avdeev[c]

[a]*Institute for Nanoscale Technology, University of Technology Sydney, PO Box 123, Broadway, NSW, 2007, Australia*

[b]*Institute of Materials Engineering, Australian Nuclear Science and Technology Organisation, PMB 1, Menai, NSW, 2234, Australia*

[c]*Bragg Institute, Australian Nuclear Science and Technology Organisation, PMB 1, Menai, NSW, 2234, Australia*

Corresponding author : Prof. M B Cortie, Institute for Nanoscale Technology, University of Technology Sydney, PO Box 123, Broadway, NSW, 2007, Australia. Email : michael.cortie@uts.edu.au, phone +61-2-9514-2208

The β-phase of $Au_7Cu_5Al_4$ undergoes a reversible shape-memory phase transformation, however there has been some uncertainty regarding the crystal structure or structures of the parent phase. Here we show that, under equilibrium conditions, the parent phase possesses the $L2_1$ structure between its A_P (about 79ºC) and ~630ºC, and the B2 primitive cubic structure between ~630ºC and its melting point. It melts directly from B2 into the liquid state and hence never achieves the random bcc A2 structure that has been previously mooted. Splat-cast samples of the alloy are martensitic, proving that development of equilibrium order and defect concentration are not pre-requisites for the $A \rightarrow M$ transformation to occur.

Keywords: X-ray diffraction, shape memory, order-disorder effect, intermetallic, crystal structure

1. Introduction

Although Al, Au and Cu each have the face-centered cubic (fcc) structure, they do not readily alloy with one another. The systems Al-Au and Al-Cu contain a series of intermetallic compounds, and while Au and Cu do form a continuous solid solution at elevated temperatures, this transforms to a series of ordered superstructures at lower temperatures. In the ternary Al-Au-Cu system two electron compounds, γ-phase $Au_xCu_{9-x}Al_4$ ($0<x<\sim6.5$) and β-phase $Au_xCu_{12-x}Al_4$ ($0<x<\sim7.5$) are known [1-3]. The 18 carat version of the β-phase, corresponding approximately to the stoichiometry $Au_7Cu_5Al_4$, is a shape-memory alloy (SMA) sometimes called 'Spangold' [4,5]. It is one of a family of precious metal SMAs that include AuCd [6], Au_2CuZn [7], TiPt [8], $Au_7Cu_7Al_2$ [8,9] and NiTiAu [10]. Like other SMAs, $Au_7Cu_5Al_4$ undergoes a reversible, displacive, thermo-elastic phase transformation between a parent (high temperature) phase and a martensitic (low temperature phase). The martensite start (M_s) and austenite start (A_s) temperatures in this alloy are normally in the range 20 to 30ºC and 55 to 80ºC respectively, with some variability due to the effect of thermal history [11,12].

The crystal structures of the parent and martensite phases are an important aspect of shape-memory alloy technology, since they influence the nature of the phase transformation and the usable amount of strain. Although the high temperature phase of $Au_7Cu_5Al_4$ was initially misidentified as being similar to the $L1_0$ phase formed from (Au,Cu) [4,13], it was later shown that it is a Hume-Rothery β-electron compound [14]. However, it is clear that this parent phase can exist in more than one condition. For example, samples of $Au_7Cu_5Al_4$ aged between 100 to ~150ºC have a well-developed shape-memory effect (as evidenced by significant transformation enthalpy, surface upheaval, dilatometric signal and acoustic emission), whereas samples produced by quenching from above 450ºC do not [11,14-17]. X-ray diffraction showed that the strongly transforming samples possessed a parent phase with $L2_1$ ordering [14] – a condition that we will designate here as "fully aged"- but samples that have been quenched from elevated temperatures – a condition that we will designate

here as “beta quenched” - have been reported to have the B2 structure [15] or mixtures of ordered phases of a nature intermediate between the A2, B2, $L2_1$ or DO_3 types [11,14,15,18]. Finally, metastable structures are reportedly formed when “beta-quenched” material is re-heated [18].

A schematic illustration of the A2, B2, DO_3 and $L2_1$ structures is provided in Fig. 1, in which it can be seen that all are variations of a body-centered cubic ABC_2 type packing. For the A2 structure the site occupancies of C are the same as those of A and B (*ie*. A=B=C), for the B2 (A=B)≠C while for the DO_3 (A=C)≠B. In the $L2_1$ structure A≠B≠C. In general, one of the ordering sequences A2→ B2→ $L2_1$, A2→ DO_3, A2→B2→DO_3 or A2→$L2_1$ is expected to occur with decreasing temperature in coinage metal β-phase alloys [19-21]. However, in some systems, such as AuZn or AuMn, there is no A2 and the alloy solidifies directly into the B2 structure [22,23]. The existence or absence of the A2 structure in other alloys is related to stoichiometry; for example, stoichiometric $AuAgCd_2$ is reported to go through the sequence $L2_1$→B2→A2 on heating, but in off-stoichiometric compositions there is no A2 phase and instead B2 is stable to the melting point [24].

In $Au_7Cu_5Al_4$, differential scanning calorimetry (DSC) indicates a phase change at about 630ºC [14-16,25]. It has been generally suggested [14] or assumed [15,16,25] that the structure of the β phase above 630ºC is A2, although no direct evidence of this has been hitherto provided. There is also uncertainty whether the transformation at 630˚C is first-order [25] or second-order [15,16]. If indeed it is the A2↔B2 transition occurring at ~630ºC then the B2↔$L2_1$ transition must necessarily occur at some lower temperature since the alloy is certainly $L2_1$ ordered at 100°C [14]. Battezatti *et al*. could find no evidence for the formation or dissolution of $L2_1$ and concluded that it was of a gradual, second-order nature and not readily detectable by DSC. On the other hand, they concluded that material quenched from 630ºC had the B2 structure and would transform exothermically and

irreversibly to $L2_1$ at 130ºC during the first reheat cycle [15]. Similarly, Gu *et al.* found inflections between 290 to 430ºC on cooling curves, which they attributed to the $B2 \rightarrow L2_1$ transition [16,25].

The structure of *beta-quenched* samples presents a further difficulty. It is known that if the ordering temperature of a non-ferrous alloy (*eg*. Cu-Al-Mn) is sufficiently high, for example above 500°C, then not even quenching can suppress subsequent binary or ternary ordering [26]. However, it is not expected in these cases that the ordering would reach the equilibrium state. In support of this, it is noted that many SMAs that have been freshly beta-quenched either do not transform to martensite, or transform weakly or differently in comparison to samples that have been well aged (*e.g.*[27-29]). The suppression of the transformation may be due in some instances to the effect of quenched-in vacancies or in others to the necessity for some minimum degree of ordering to be present.

Jin *et al*. examined $Au_7Cu_5Al_4$ quenched from 680ºC and concluded [18] that it ordered to DO_3 rather than $L2_1$ when re-heated up through the range 172 to 281ºC. A depression of the M_s from about 0ºC to -35ºC was attributed to the presence of this DO_3 parent. The structure above 630°C was believed to be A2. Battezatti *et al.* [15] showed that when $Au_7Cu_5Al_4$ was rapidly solidified onto a copper wheel, and not allowed to cool below 17°C, it consisted of a partially transformed mixture of $L2_1$ phase and martensite. It transformed back to parent phase on heating with an enthalpy of only 1.1 J/g (compared to the usual 3 to 3.5 J/g [15,30]). The lower enthalpy was attributed to the lower volume fraction of martensite present. However, a sample that had been beta quenched from 630°C appeared to consist of only the B2 phase.

Clearly, the structure of the β-phase at higher temperatures, and the results produced by quenching it, have remained uncertain. Here we have used *in situ* X-ray and neutron powder diffraction studies to resolve these uncertainties.

2. Material and methods

The samples for this project were manufactured using high purity base metals of Au (99.99%), Cu (99.9%) and Al (99.99+%) melted in an alumina crucible under a protective layer of carbon pellets. The Au was melted first, and then the Cu and Al stirred in. The samples were annealed at 700°C to convert them into β-phase, followed by quenching into iced brine. Gravity splat-cast samples (GSC) were produced by either being poured in the molten state onto a cold refractory plate (GSC1) or onto a copper plate (GSC2), whereas impact splat cast (ISC1 and ISC2) samples were made by dropping a copper block onto a molten bead of the alloy. Samples GSC1, GSC2 and ISC1 were peeled off their respective substrates and not cooled below -5ºC prior to analysis. In contrast, sample ISC2 was immediately stored into liquid nitrogen after solidification but then reheated to room temperature three hours later for X-ray diffraction.

DSC analyses were performed using a Thermal Analysis DSC 2920 with a ramp rate of 10°C/min. Samples were also pulverized in a ring-mill for diffraction studies, and annealed at 500ºC for 1 to 3 hours to remove strain. Mössbauer spectroscopy was performed at 4 K using an activated Au source and a transmission configuration.

Powder diffraction was undertaken at the Australian Synchrotron (10BM1: Powder Diffraction) on spinning 0.3 and 0.5 mm capillaries filled with $Au_7Cu_5Al_4$ powder between room temperature and 800 °C. Synchrotron data were collected from a LaB_6 Standard (NIST 660a) to accurately calibrate the wavelength and determine the instrument contributions to the observed line profiles. Samples were analyzed at an incident wavelength of 1.12715 ± 0.00001 Å (0.5 mm capillary) and 1.15970 ± 0.00001Å (0.3 mm capillary) as these provided the best peak shape and peak-to-background ratio within the available energy range of the instrument. X-ray patterns of bulk samples were obtained on laboratory machines using either Cu-k_α or Mo-k_α radiation. Due to the large grain size of the material, the patterns of the bulk samples were strongly effected by texture.

While the overall structure is already known to be based on body-centered cubic packing, determination of the site occupancies is crucial to determine the actual crystal structure type. The X-ray patterns are dominated by the scattering length of the Au component. Hence, in order to resolve the site occupancies, complementary neutron powder diffraction data were collected on Echidna (the high resolution powder diffractometer) at the OPAL reactor at ANSTO in Australia because neutron diffraction is more sensitive to the Al positions in this system (see later). Data were collected from stationary powder samples at 200, 550 and 700 °C using a neutron wavelength of 1.5388 Å.

An estimate of the lattice occupancy was made using a Pascal script running within Crystallographica[1] that iterated through the permutations of occupancy of Au, Al and Cu on the A, B and C sites of a notional ABC_2 Heusler-type arrangement adjusted for the actual stoichiometry of $Au_7Cu_5Al_4$. The suitability of a permutation was judged by calculating the ratios of selected superlattice and fundamental peaks on the patterns. In particular, the {111} peak, which is generated by ternary ordering of the $L2_1$ or DO_3 types, was assessed relative to the fundamental body centered cubic {220} and {422} peaks, while the {200} and {420} peaks, which are generated by binary ordering of the B2 type [14], were assessed relative to the {220} and {422} respectively. Use of more than one peak to estimate the ordering provided a means of reducing the effects of any texturing (preferred orientation) in the sample. The algorithm used (see Supporting Data for the script) searched for the minimum value of the parameter, *s*:

$$s = (I_{111}/I_{220}\text{-}I_{111M}/I_{220M})^2 + (I_{111}/I_{422}\text{-}I_{111M}/I_{422M})^2 + (I_{200}/I_{220}\text{-}I_{200M}/I_{220M})^2 + (I_{420}/I_{422}\text{-}I_{420M}/I_{422M})^2$$

where I_{xxx} is the calculated height of the indicated peak, and I_{xxxM} is the measured area of that peak. The effect of thermal vibration was ignored. The calculation was repeated for both X-ray and neutron data and the average value of *s* for the two radiations used to drive the optimization using the method of steepest descent.

[1] Crystallographica is a product of Oxford Cryosystems Ltd, of 3 Blenheim Office Park, Lower Rd, Long Hanborough, Oxford OX8 8LN, UK.

3. Results and Discussion

3.1. Absence of the A2 structure

During heating from low temperatures, the martensite of $Au_7Cu_5Al_4$ transforms into the high temperature parent phase by a displacive, first-order phase transformation. The transition occurs between 55 and 85°C, depending on prior thermal history [11]. The martensite has a relatively complex crystal structure, which is easily recognizable on the diffraction patterns, but we will not discuss it further here.

A series of parent phase diffraction patterns at temperatures from 100°C upwards is shown in Fig. 2. The {220} peak is one of the fundamental peaks of the underlying body-centered cubic lattice and is always present, whereas the presence of a well-developed {200} peak indicates that binary ordering of the B2 type has occurred. The {111} peak is visible on patterns taken from 100ºC to about 600ºC, but is always considerably lower in height here than the {200}. In general, the presence of the {111} and {311} peaks indicates either binary DO_3 or ternary $L2_1$ ordering, but the relationship of peak heights in the present case ($I_{220M} >> I_{111M}$) shows that the ordering must be of the $L2_1$ type [14].

Fig. 3 shows the sum of the peak areas of the first three fundamental bcc A2 reflections ({220}, {400} and {422}), the sum of the first three B2 reflections ({200}, {222} and {420}) and the sum of the first two reflections due to ternary ordering ({111} and {311}) plotted from 300 to 800°C. Summing the peaks in this way helps reduce effects due to crystallographic texture in the sample. Loss of the $L2_1$ ordering on heating through about 620ºC is evident. The transition starts at temperature *a* and ends at *b*. Melting of the material is indicated by the drastic decline in peak intensity between temperatures *s* and *l*, corresponding to solidus and liquidus respectively. It is important to note that the peaks due to B2 ordering retain their intensity up to the liquidus. The overall decrease in peak intensity with increase in temperature in Fig. 3 is due to increase in thermal

vibration. It is clear from these plots that the material is $L2_1$-ordered from the A_s up to about 620ºC, and B2-ordered from about 620ºC to the melting point. The recent reports [15,16,25] in the literature of the existence of the A2 structure or of various phase transformations from A2 to $L2_1$ or DO_3 need to be re-visited in the light of these results.

3.2. Lattice occupancies and cell parameters

The overall pattern of the parent phase between 80 and 630°C can be indexed as a face-centered cubic structure, with the space group Fm3m. However, examination of the effect of possible permutations on occupancy on the calculated diffraction pattern showed that the X-ray pattern could, in principle, be generated by more than one arrangement of atoms (Fig. S1a, Supporting Information), whereas simulations made using neutron radiation indicated a single, but extended, range of possibilities (Fig. S1b, Supporting Information). Fortunately, consideration of the X-ray and neutron data *simultaneously* shows that the only possible common solution has an Au occupancy on the C site of about 0.8 and an Au occupancy on the B site of nearly zero (Fig. S1c, Supporting Information). In both cases, the Al of this common solution is found to be concentrated on the B site. The details of the X-ray pattern are most sensitive to the location of the Au atoms, Fig. 4, as the atomic number of Au (79) is considerably greater than that of Al (13) or Cu (29). In contrast, optimization of occupancy against the neutron pattern was not very sensitive to the Au and Cu occupancies because they have rather similar neutron scattering cross-sections (7.32 vs. 7.49 barns respectively). In this case it was more useful to optimize the structure with respect to Al content (because the coherent scattering cross section of that element (1.50 barns) is quite different to Au or Cu. The best solution (Fig. S2a and c, Supporting Information) has an Al occupancy of about 0.90 to 0.95 in the B site and negligible amounts elsewhere.

The best-fitting occupancies taken by considering the X-ray and neutron data simultaneously are listed in Table 1 for data collected at 200, 550 and 700ºC. The starting guess for the steepest-descent

algorithm was an Au occupancy of 0.8 in the C site and none in the B site, and 0.8 Al in the B site and none in the A site. (The other occupancies can be calculated from these values by reference to the stoichiometry of the alloy). Given that the starting patterns were influenced by some texture, we estimate that the occupancy values in the Table are not more accurate than ±0.05. Nevertheless, it can be seen that the lattice at 200ºC has slightly better developed $L2_1$ ordering than the one at 550ºC, and that the ordering on the A site decreased slightly as the temperature was varied from 200 to 700ºC. The diffraction patterns calculated by this optimization method are compared to measured ones in Fig. 5 for data taken at 200°C. A similar quality of fit was obtained at other temperatures.

The synchrotron data is severely affected by absorption. Even with a 0.3 mm sample diameter the μr is ~6. Working with the true integrals shows that this gives rise to an intensity reduction across the pattern of ~99.7% at zero to ~98% at 90º, a peak shift (of centroid) from 0º at 0º to ~+.012º at 20º reducing to ~+.007º at 90º, and a reduction in the sample contribution to the peak width of ~96% at 20º to ~70% at 90º with an associated shape change to an asymmetric triangle. While various empirical approximations are available for the intensity variation and the width variation can be taken care of with adjustments to the U and W parameters, none of Rietica, GSAS or FULLPROF[2] have satisfactory approximations for the peak shift or shape change. As a consequence we have not yet been able to perform the final Rietveld refinements of the synchrotron data or perform joint Rietveld refinements with the neutron data. However the relative changes in lattice parameter and thermal parameters with temperature can be used to demonstrate features of the data. The Rietveld refinements will be the subject of a separate paper.

It is clear, however, that a significant phase transition occurs at 630°C, in which atoms randomize on the A and B sites, forming a primitive cubic phase, B2. An example of the refinement for the $L2_1$ and B2 materials is given in Fig. 6, for data collected at 541 and 720ºC respectively. The space group of

[2] RIETICA, GSAS and FULLPROF are free utilities available from http://www.rietica.org, http://www.ncnr.nist.gov/xtal/software/downloads.html and http://www.ill.eu/sites/fullprof respectively.

the 720°C data is Pm3m, and the lattice parameter is 3.132 Å. There are two sites present in this structure, the Au-rich site (x=0.0, y=0.0, z=0.0), and the other site (x=0.5, y=0.5, z=0.5) with random ordering of the remaining elements. The odd reflections present show that the high temperature phase is primitive cubic. As mentioned, the intensity of the peaks during a heating scan start to drop off at ~730ºC, indicating that melting is taken place. The B2 phase was retained through to the last vestiges of solid material to melt, disproving the assumptions made in the previous literature [15,16,25] of a high temperature A2 structure.

3.3 Removal of lattice strain

Although the powdered samples had been annealed prior to the synchrotron experiment, transformation from martensite into the parent phase generates new strain, of the order of 2 to 4% [31]. When this annealed out during the heating scan, there was a corresponding increase in peak height, Fig. 7 (upper curves). It is evident that the stresses were annealed out at by about 300°C for the 220 but in some directions the height did not maximize until ~400°C. The overall area under the peaks Fig. 7 (lower lines), however, only showed the expected monotonic decline due to increased thermal vibration, indicating that no change in volume fraction of the parent phase had occurred. However during the cooling scans, Fig. 7, there were increases in peak heights at different rates for different reflections which requires further explanation. Similar results were obtained for the 0.5 mm capillary.

3.4 B2/$L2_1$ transition

The lattice parameter for the two parent phases ($L2_1$ and B2) is plotted as a function of temperature in Fig. 8. It can be seen that there is a marked change in slope at ~630ºC, but no discontinuity, factors which taken together with the DSC data (lambda shape of curve and lack of undercooling, inset to Fig. 8) tend to indicate that this is a second-order transition, *cf.* Obrado [19] and Battezzati

[15]. The trends in the lattice parameter data match those of the thermal contraction data of Jin *et al*. [25], which are also shown on Fig. 8.

3.5 Structure of beta-quenched material

As we have shown here, solid $Au_7Cu_5Al_4$ has the B2 structure at temperatures above 630°C so any transitions observed in beta quenched material must begin from the B2 phase. Therefore, the transformation observed by Jin *et al.* [18] could only have been a B2→DO_3 transition and not an A2→DO_3 transformation. It is reported that the A2→DO_3 and B2→DO_3 transformations are almost inevitably first-order for reasons relating to symmetry [19] so if DO_3 phase did precipitate it should be apparent in microstructural sections or diffraction patterns. The associated internal friction and electrical resistivity changes previously observed in the 200 to 400°C range[16,18,25] need further investigation. However, the present results clearly show that these changes must be due to short, rather than long range ordering, since they are not shown in our X ray diffraction patterns.

The X-ray diffraction patterns of three of these samples are compared in Fig. 9 to patterns obtained in the synchrotron for 'equilibrium' powders of martensite and parent phase. The patterns of the splat-cast samples are of comparatively poor quality, as the newly solidified foil was placed directly onto the stage of the X-ray machine, with no other specimen preparation. The patterns would therefore be expected to show the effects of preferred orientation, surface oxides, and lack of flatness. Nevertheless, it is clear that samples ISC1 and ISC2 were martensitic at the time of their first measurement. Furthermore, there is no evidence that aging of these samples (for 72 hours at room temperature, and about one week at temperatures between 20 and 60ºC respectively) changed this martensite, and such differences as there are between the four patterns may be attributed to sampling and/or instrumental factors. The ISC2 sample underwent a well-developed transition to austenite when reheated, with an A_p of 79± 0.5ºC, and this was not changed by a subsequent heat treatment at 200ºC, Fig.10. On the other hand the GSC2 sample appeared to have contained little

martensite in the as-cast condition, but had certainly developed the characteristic split peaks of martensite after several weeks of aging at room temperature. Clearly, the splat-cast microstructure of $Au_7Cu_5Al_4$ is acutely sensitive to cooling rate, with the GSC2 sample here, and the samples of Battezatti (copper wheel) and Levey (water-cooled copper hearth), having been cooled sufficiently fast to suppress the M_S to below the temperature of the quench medium. However, it appears that there is a time-dependent process that gradually raises the M_S of such β-phase samples so that they convert to martensite at room temperature after several weeks.

Thermal analysis of a portion of sample GSC1 that had been freshly re-beta-quenched from 700ºC and quenched into iced brine [11] failed to show an A_S, indicating that the M_s was well below 0ºC when in this condition. However, after such a beta-quenched sample was aged at 150ºC then quenched again into iced brine, thermal analysis indicated an A_S at 81.5ºC. A further martensitic stabilization treatment of such material at 60ºC for 17 hours resulted in an A_S of 84.6ºC. This is evidence that, provided it has received a prior aging treatment in the 140 to 450ºC range, $Au_7Cu_5Al_4$ is only slightly susceptible to the phenomenon of 'martensite stabilization'.

The results of applying Mössbauer spectroscopy to the GSC1 splat-cast foil of the 5.8 wt% Al alloy after two years of aging at room temperature, and to pure gold, are listed in Table 2 and shown in Fig. 11. The absorption spectrum of the alloy displayed the same inverted Gaussian shape as for pure gold, but the minimum was shifted (the isomeric shift) by +3.21 mm/s. No quadropole splitting was visible, implying that the gold atoms in this sample were in an approximately cubic configuration and that the gold in the sample was present in a single phase, at least to within the resolution of the measurements. However, the line widths for the two measurements are comparatively large (for comparison, measurements in the literature for Au and AuCd show line widths in the range 1.90 to 2.50 mm/s depending on microstructure [32,33]), implying that an excessive specimen thickness or some other experimentally-derived source of noise is obscuring the data in the present instance. The

isomeric shift of the experimental alloy with respect to pure gold is caused by a changed electronic state of the Au atoms, due especially to the fact that their nearest neighbors are no longer all Au atoms. Since gold is noble (electronegative), the introduction of an electropositive metal into the lattice tends to decrease the electronic charge around the gold atoms, thereby causing the isomeric shift.

4. Conclusions

The $Au_7Cu_5Al_4$ alloy does not achieve the fully randomized A2 structure at any stage, in contrast to previous reports or suggestions. The highest temperature solid phase has the B2 (primitive cubic) structure. It appears that the B2 structure transforms to $L2_1$ on cooling through ~630ºC, and that this transition is second-order in nature. The lattice parameters and chemical occupancy of the parent phase have been estimated. The reversion of martensite to parent phase during a heating scan generated strain, but this effect was annealed out by about 400°C. Splat-cast samples of $Au_7Cu_5Al_4$ are martensitic if cooled below the M_s, but can be retained in the parent phase condition by keeping the minimum sample temperature above the M_S.

Acknowledgements

This research was undertaken on the Powder Diffraction beamline at the Australian Synchrotron, and on the Echidna neutron diffraction beamline of the OPAL reactor at the Australian Nuclear Science and Technology Organization. The views expressed herein are those of the authors and are not necessarily those of the owner or operator of the Australian Synchrotron or OPAL. The DSC scan inset in Figure 7 was originally kindly run by Mettler-Toledo of Switzerland and originally published in Levey *et al*. [17]. The Mössbauer data were provided by the late Prof. Herman Pollock of the University of Witwatersrand, Johannesburg, South Africa and his colleagues Dr. Gio Hearne and Mr. Seda Takele.

References

[1] F. C. Levey, M. B. Cortie, L. A. Cornish, A 500°C isothermal section for the Al-Au-Cu system, Metall. Mater. Trans. A. 33A (2002) 987-994.

[2] V. K. Bhatia, C. S. Kealley, A. Dowd, F. C. Levey, M. B. Cortie, The aluminium-copper-gold ternary system, Gold Bull. 42(3) (2009) 201-208.

[3] V. K. Bhatia, C. S. Kealley, R. Wuhrer, K. S. Wallwork, M. B. Cortie, Ternary β and γ phases in the Al-Au-Cu ternary diagram, J. Alloys Compd. 488 (2010) 100-107.

[4] I. M. Wolff, M. B. Cortie, The development of Spangold, Gold Bull. 27(2) (1994) 44-54.

[5] M. Cortie, I. Wolff, F. Levey, S. Taylor, R. Watt, R. Pretorius, T. Biggs, J. Hurly, Spangold, a jewellery alloy with an innovative surface finish, Gold Technol. 14 (1994) 30-36.

[6] L. C. Chang, T. A. Read, Plastic deformation and diffusionless phase changes in metals - The gold-cadmium beta-phase, Trans. AIME 191 (1951) 47-52.

[7] G. B. Brook, R. F. Iles, Gold-copper-zinc alloys with shape memory, Gold Bull. 8(1) (1975) 16-21.

[8] T. Biggs, M. B. Cortie, M. Witcomb, L. A. Cornish, Martensitic transformations, microstructure and mechanical workability of TiPt, Mater. Trans A 32A (2001) 1887-1902.

[9] Y. Isobe, Form retaining alloy, Japanese Patent JP 2267237 (1991).

[10] S. Besseghini, F. Passaretti, E. Villa, P. Fabbro, F. Ricciardi, Gold with a martensitic transformation: which opportunities?, Gold Bull. 40(4) (2007) 328-335.

[11] F. C. Levey, M. B. Cortie, L. A. Cornish, Displacive transformations in Au - 18 wt% Cu - 6 wt% Al, Metall. Mater. Trans. A. 31 (2000) 1917-1923.

[12] S. Urbano, A. Manca, S. Besseghini, G. Airoldi, Martensite ageing effects in $Au_7Cu_5Al_4$, Scr. Mater. 52(4) (2005) 317-321.

[13] H. Sato, R. S. Toth, Effect of additional elements on the period of CuAuII and the origin of the long-period superlattice, Phys. Rev. 124(6) (1961) 1833-1847.

[14] M. B. Cortie, F. C. Levey, Structure and ordering of the 18-carat Al-Au-Cu β phase, Intermetallics 8(7) (2000) 793-804.

[15] L. Battezzati, G. Fiore, M. Massazza, A shape memory gold alloy processed by rapid solidification, J. Alloys Compd. 434/435 (2007) 264-267.

[16] Y. Gu, M. Jin, X. Jin, A2 / B2 / $L2_1$ ordering transitions in Au–Cu–Al alloys, Intermetallics 17(9) (2009) 704-709.

[17] F. C. Levey, M. B. Cortie, L. A. Cornish, Determination of the 76 weight % Au section of the Al-Au-Cu system, J. Alloys Compd. 354 (2003) 171-180.

[18] M. Jin, J. Liu, X. Jin, Ordering transitions in quenched $Au_7Cu_5Al_4$ alloy and effect of order on martensitic transformation, Intermetallics 18(5) (2010) 846-850.

[19] E. Obrado, C. Frontera, L. Manosa, A. Planes, Order-disorder transitions of Cu-Al-Mn shape-memory alloys, Phys. Rev. B 58 (1998) 14245.

[20] M. H. Wu, C. M. Wayman, On the interpretation of long range order in Cu-Zn-Al shape memory alloys, Scr. Metall. Mater. 25 (1991) 1633-1640.

[21] T. Makita, M. Kobukata, A. Nagasawa, J. Mater. Sci. 21 (1986) 2212.

[22] A. Prince, G. V. Raynor, D. S. Evans, Phase Diagrams of Ternary Gold Alloys. The Institute of Metals, London, 1990.

[23] B. H. Chen, H. F. Franzen, J. Less Comm. Metals 143 (1988) 331.

[24] T. Suzuki, S. I. Nakamoto, nfluence of quenching on the martensitic transformation temperature in Au-47.5 at% Cd-Ag alloys, Mater. Sci. & Eng. A 273 (1999) 549-553

[25] M. J. Jin, Y. J. Gu, X. Jin, Characterization of ordering transitions in Au–Cu–Al alloys, Mater. Charact. 60 (2009) 1395-1399.

[26] Y. Sutou, T. Omori, R. Kainuma, K. Ishida, Ductile Cu–Al–Mn based shape memory alloys: general properties and applications, Mater. Sci. Technol. 24(8) (2008) 896-901.

[27] J. D. Stice, C. M. Wayman, Metall. Trans. A 13 (1982) 1687.

[28] R. Romero, A. Somoza, M. A. Jurado, A. Planes, L. Mañosa, Quenched-in defects and martensitic transformation in Cu-Al-Be shape memory alloys, Acta mater. 45(5) (1997) 2101-2107.

[29] T. Makita, A. Nagasawa, Scripta Metall. 18 (1984) 1275.

[30] L. Fumagalli, S. Besseghini, F. Passarett, G. Airoldi, Thermoelastic martensitic transformation in Au-Cu-Al alloys doped with Co or Ir, J. Alloys Compd. 433 (2007) 332-337.

[31] M. B. Cortie, F. C. Levey, Formation, modulation and adaptive twinning of martensite in the $Au_7Cu_5Al_4$ shape memory system, Intermetallics 10 (2002) 23-31.

[32] J. A. Sawicki, B. D. Sawika, Conversion electron Mössbauer spectra of very thin gold films, Hyperfine Interact. 16(1-4) (1983) 1013-1016.

[33] J. D. Cashion, J. Chadwick, C. M. Coyle, T. R. Finlayson, The aging effect in Au-Cd alloys: A Mössbauer spectroscopy study, J. Phys. IV France 112 (2003) 1087-1090.

Tables

Table 1. Best-fitting solutions to lattice occupancy of $Au_7Cu_5Al_4$ β phase at various temperatures obtained by iteration over possible permutations of occupancy in *Crystallographica*. Accuracy of entries estimated to be not better than 0.05 due to residual texture effects in samples.

	site	A	B	C
200ºC	Au	0.07	0.06	0.80
	Al	0.00	0.94	0.02
	Cu	0.93	0.00	0.18
550ºC	Au	0.16	0.07	0.76
	Al	0.16	0.82	0.00
	Cu	0.68	0.12	0.25
700ºC	Au	0.74	0.13	-
	Al	0.00	0.48	-
	Cu	0.26	0.39	-

Table 2. Mössbauer parameters for Au and $Au_7Cu_5Al_4$.

Parameter	Au	$Au_7Cu_5Al_4$
Shape	simple inverted Gaussian	simple inverted Gaussian
isomeric shift	-1.05 mm/s	+2.16 mm/s
line width	2.60	2.52
area	0.21	0.23

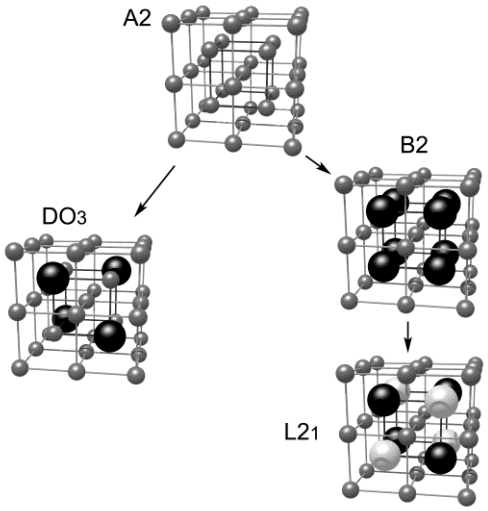

Fig. 1. Chemical ordering of the A2, B2, $L2_1$ and DO_3 structures. The atoms in each case are packed in a body-centered cubic fashion but symmetries differ. All sites are equivalent in A2, which is body-centered cubic. Further ordering of A2 can produce DO_3 or B2 structures, by either first- or second-order processes. DO_3 has face-centered cubic symmetry whereas B2 can be considered to be made up of two interpenetrating simple cubic lattices. Further ordering of B2 to $L2_1$ phase is possible in ternary systems by a second-order (homogenous) process, however conversion of DO_3 to $L2_1$ or vice versa would normally be expected to be a first order or heterogeneous transformation.

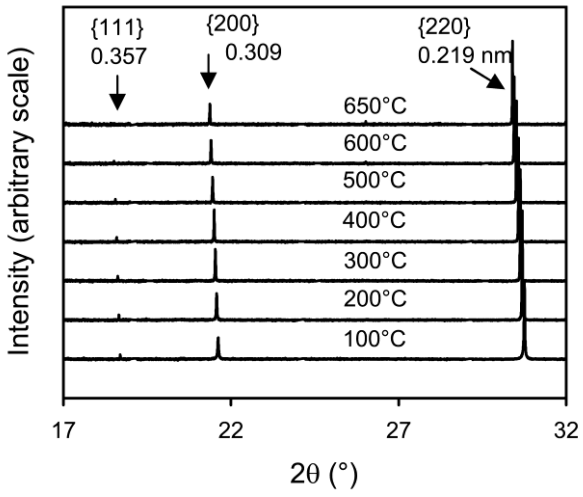

Fig. 2. Portion of synchrotron X-ray diffraction pattern, with scans taken over a range of temperatures, showing the presence of the {111} and {200} peaks associated respectively with ordering of the ternary ($L2_1$) and binary (B2) types, and the fundamental {220} peak associated with the underlying body-centered cubic lattice. The peak positions in nm are for the 100ºC data.

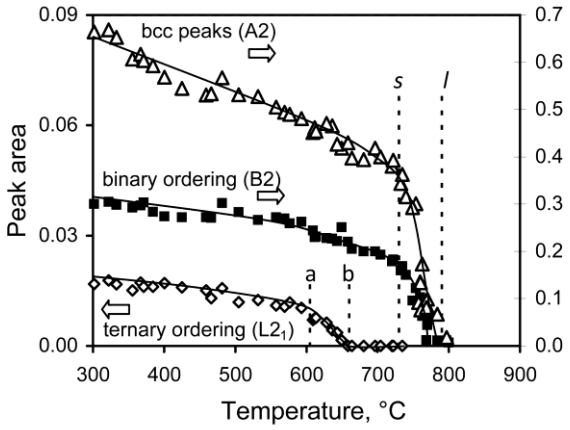

Fig. 3. Effect of temperature on diffraction peaks caused by ternary, binary and no ordering (0.5 mm capillary). Trend lines are merely to guide the eye. Relevant vertical axes for data sets indicated by arrows. It is clear that the $L2_1$ phase transforms to B2 between points *a* and *b* and that the sample melts between solidus (*s*) and liquidus (*l*).

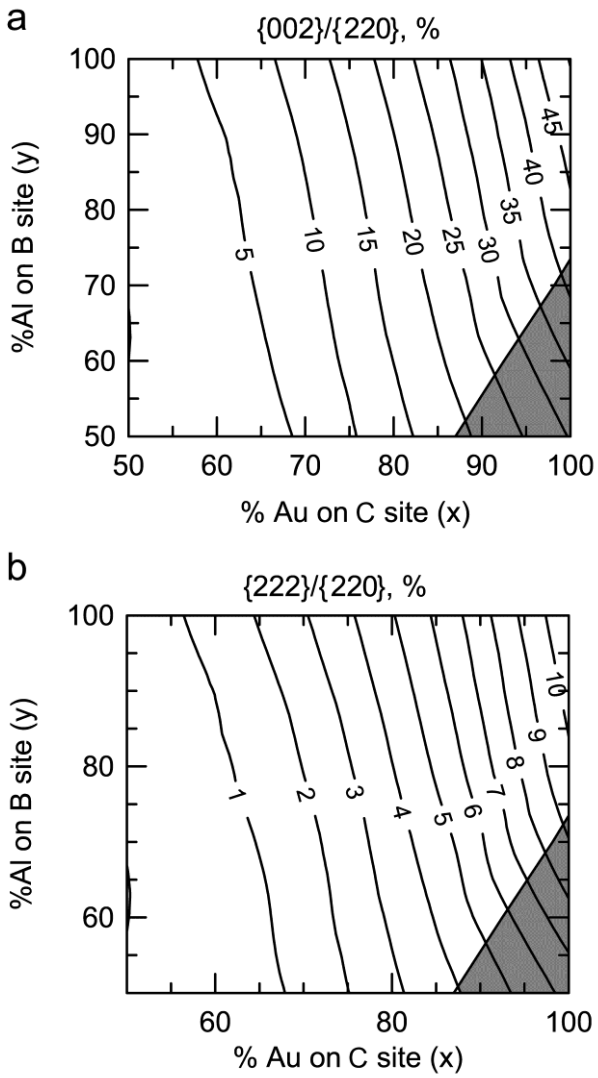

Fig. 4. Effect of distribution of Au and Al atoms on (a) ratio of {200} peak height to {220} peak height, (b) ratio of {222} to {220} peak height. The shaded regions are not possible with the stoichiometry of $Au_7Cu_5Al_4$. The Au occupancies exert a dominant effect on the X-ray diffraction pattern.

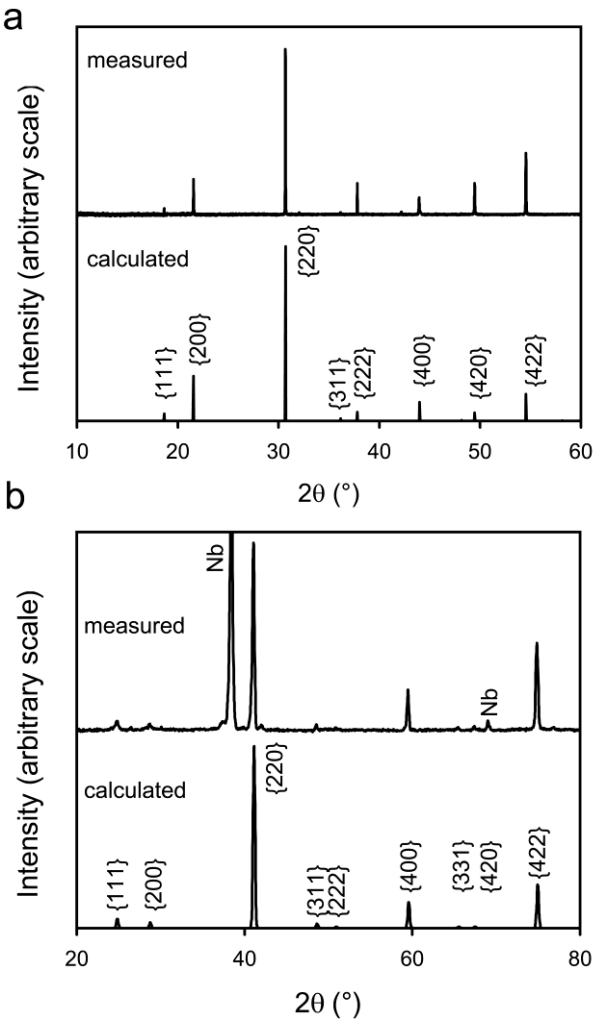

Fig. 5. Best-fitting simulations of the X-ray and neutron diffraction patterns obtained at 200ºC. The neutron diffraction pattern also contains niobium peaks from the furnace.

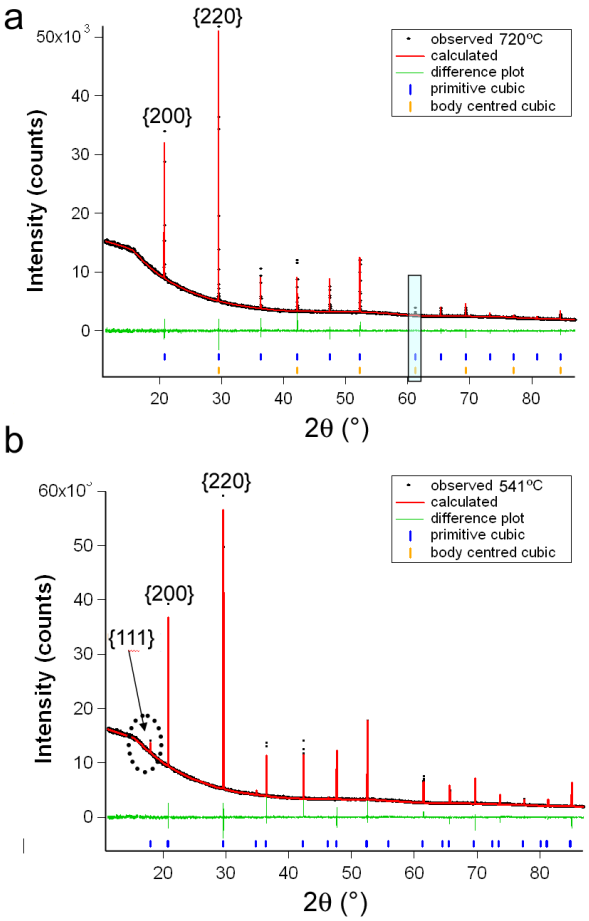

Fig. 6. Rietveld refinement of the synchrotron powder diffraction data collected at 720 ºC and 541 °C (the blue box is an excluded region, as half of the reflection has fallen into the detector gap). The {200} peak of the B2 phase is clearly visible at both temperatures, while the {111} peak generated by ternary ordering is absent at 720 °C.

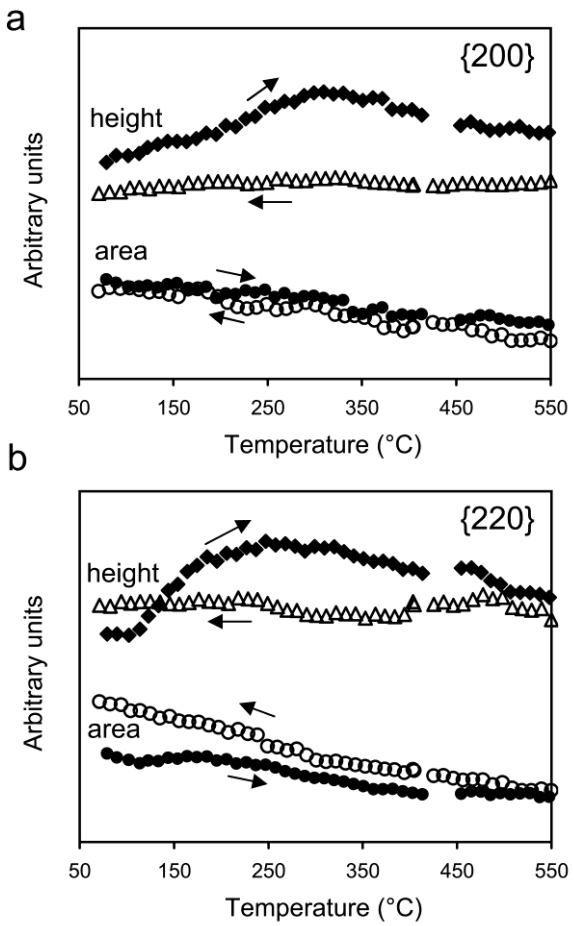

Fig. 7. Change in height and area of a) {200}, a peak generated by B2 ordering, and b) {220}, a fundamental body-centered cubic peak. In each case the heating part of the scan is associated with an increase in peak height up to about 300°C. In contrast, the area under the peaks appears to be influenced only by thermal vibration.

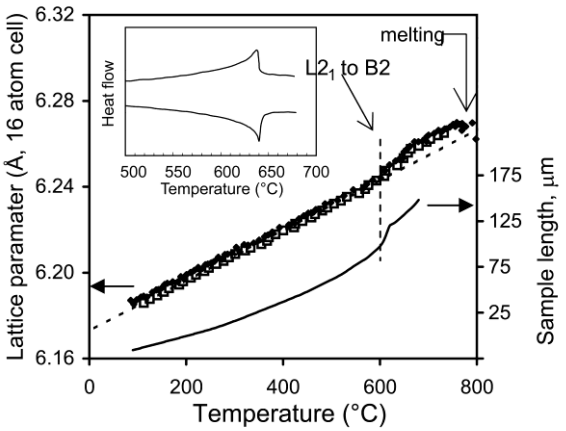

Fig. 8. Lattice parameter as a function of temperature determined from a refinement of the synchrotron data (hollow squares) and independently from the peak positions using the expression $a=d_{hkl}*\sqrt{(h^2+k^2+l^2)}$ (closed diamond symbols) (note: B2 primitive cell value doubled for ease of plotting). Also shown is the thermal contraction data of Jin *et al*., obtained by digitizing their Figure 1 [25]. There is a change in the lattice parameter and sample length at 630ºC, corresponding to the $L2_1 \leftrightarrow B2$ transformation. The forward and reverse heat flows measured in this alloy for this transformation are shown as an inset, reproduced with permission from Levey et al.[17]. The thermal signal shows the classic shape of a second-order phase transformation[19].

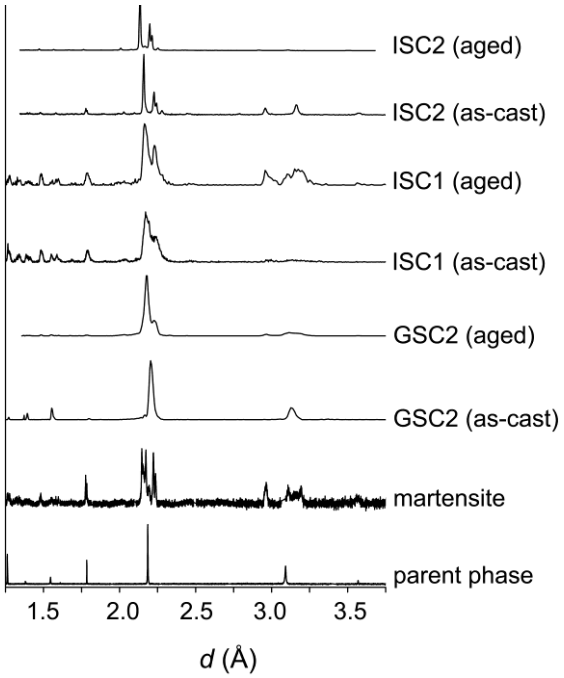

Fig. 9. X-ray diffraction patterns of three splat-cast samples and two standard samples, showing that most of the splat-cast samples were martensitic. The exception is sample GSC2, which appears to have been substantially comprised of B2 phase immediately after solidification. Different radiations have been used, so the data have been plotted against interplanar spacing, *d*, for the purposes of comparison. (The radiations used were: ISC2 - Cu Kα , ISC1 - Mo Kα, GSC2 - Cu Kα, typical martensite - synchrotron 1.12715 Å, typical parent phase - synchrotron 1.53878 Å.

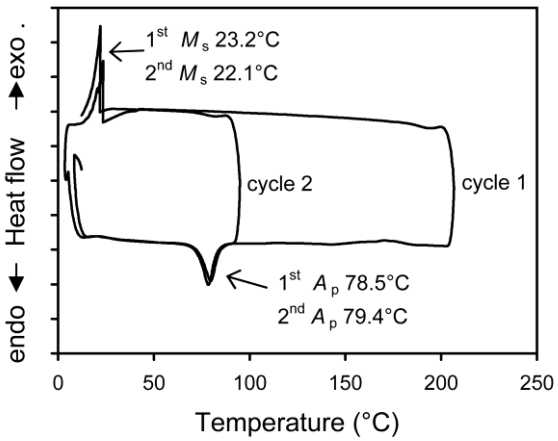

Fig. 10. Thermal analysis of splat-cast sample ISC2, after two days aging at room temperature, showing that it was fully capable of reverting to parent phase.

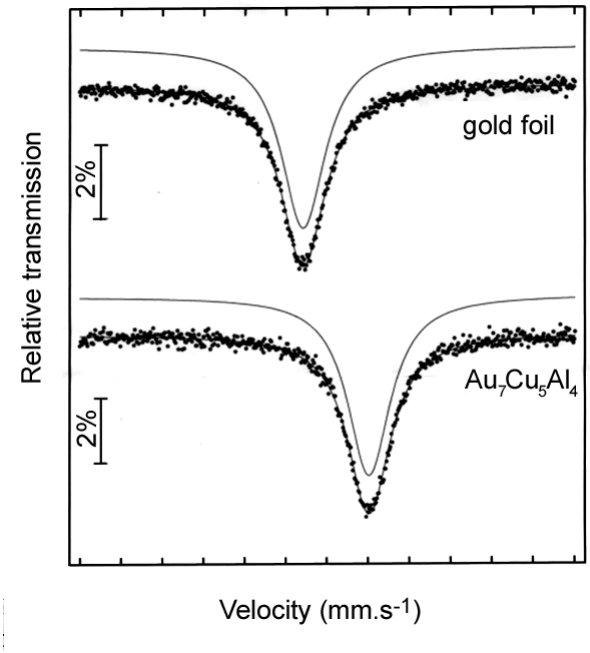

Fig. 11. Mössbauer spectra for foils of pure gold and $Au_7Cu_5Al_4$ indicating an approximately cubic symmetry for the gold atoms and a pronounced isomer shift for the alloy relative to pure gold.

Supporting Information

1. Pascal script for Crystallographica[3] program.

This algorithm searches for the best-fitting occupancy by matching calculated peak heights for X ray and neutron patterns against the experimentally obtained peak heights. It is set up to work specifically with the stoichiometry of $Au_7Cu_5Al_4$ but can be modified for other substances.

```
{program DUAL_ITERATE}
{looks for best composition, uses both x ray & neutron}

var II, JJ ,KK, LL: integer;
var A_Au,B_Au,C_Au,A_Al,B_Al,C_Al,A_Cu,B_Cu,C_Cu: real;
var A_Au1, B_Au1, B_Al1, C_Al1 : real;
var STEP : real;
var A_Au_x,A_Al_x,A_Cu_x,B_Au_x,B_Al_x,B_Cu_x,C_Au_x,C_Al_x,C_Cu_x : real;
var Au, Al, Cu : real; {used to pass value to SET}
var OLDERROR,ERROR,ERRORX, ERRORN : real;
var FOREVER : boolean;

var I0_111,I0_002,I0_RAT1, I0_RAT2 : real; {ratios from experimental data}

procedure SET(SITE : string);
var
  LABEL : string;
begin
  LABEL:="Au"+SITE;
  SetOccupancy(LABEL,Au);
  LABEL:="Al"+SITE;
  SetOccupancy(LABEL,Al);
  LABEL:="Cu"+SITE;
  SetOccupancy(LABEL,Cu);
end;

function ALLOCATED: boolean;
begin
  {add in missing ones, this stoichiometry is for Spangold}
  C_Au:=(0.435-(8*A_Au+4*B_Au)/16)*4;
  A_Al:=0.243*2-0.5*(B_Al+C_Al);
  A_Cu:=1-A_Au-A_Al;
  B_Cu:=1-B_Au-B_Al;
  C_Cu:=1-C_Au-C_Al;

  if (C_Au<0)or(A_Al<0)or(C_Al<0)or(A_Cu<0)or(B_Cu<0)or(C_Cu<0) then ALLOCATED:=false
  else
  begin
    {A sites}
    Au:=A_Au; Al:=A_Al; Cu:=A_Cu;
    SET("1");
    SET("4");
    SET("5");
    SET("7");
    SET("2");
    SET("3");
    SET("6");
    SET("8");

    {B sites}
    Au:=B_Au; Al:=B_Al; Cu:=B_Cu;
    SET("9");
    SET("12");
    SET("14");
    SET("15");

    {C sites }
    Au:=C_Au; Al:=C_Al; Cu:=C_Cu;
    SET("10");
```

[3] Crystallographica v1.60c is a product of Oxford Cryosystems

```
    SET("11");
    SET("13");
    SET("16");

    ALLOCATED:=true;
  end;
end;


procedure CALCFIT;

var I111,I002,I022,I024,I224 : real;
var RAT1,RAT2 : real;
var h,k,l : array[1..1] of integer; {will be dynamically sized}
var d,i : array[1..500] of real; {will be dynamically sized}
var n   : integer;
{var count : integer;}

begin
  PowderReflections(h,k,l,d,i,n); {loads arrays with data}
  {for count:=1 to n do
    if i[count]>0.001 then writeln("#",count:6,h[count]:6,k[count]:6,l[count]:6,d[count]:10:4,i[count]:15:4); }


  {these only work for default powder ranges.. recheck arrays above if in doubt}
  I111:=8*i[19]; {sum intensities to get peak heights, using multiplicity}
  I002:=6*i[27];
  I022:=12*i[81];
  I024:=24*i[365];
  I224:=24*i[461];

  {calc ratios}
  I111:=I111/I022;
  I002:=I002/I022;

  RAT1:=I111/I224;
  RAT2:=I024/I224;

  ERROR:=sqr((I111-I0_111)/I0_111)+sqr((I002-I0_002)/I0_002)+sqr((RAT1-I0_RAT1)/I0_RAT1)+sqr((RAT2-I0_RAT2)/I0_RAT2);

end;


begin
  clearconsole;
  writeln("------------------");
  writeln("program Dual_Iterate");
  writeln;

  ReadCif("frame.cif"); {48 atom cell, 16 sites, 3 types of atom per site}

  write("A_Au :"); readln(A_Au1);
  writeln;

  write("B_Au :"); readln(B_Au1);
  writeln;

  write("B_Al :"); readln(B_Al1);
  writeln;

  write("C_Al :"); readln(C_Al1);
  writeln;

  writeln("step  eg 0.05 :"); readln(STEP);

  FOREVER:=false;

  repeat
    OLDERROR:=1e9;

    for II:=0 to 2 do
     for JJ:=0 to 2 do
      for KK:=0 to 2 do
       for LL:=0 to 2 do
       begin
         {build occupancy variables}
         A_Au:=A_Au1+(II-1)*STEP;
```

```
      B_Au:=B_Au1+(JJ-1)*STEP;
      B_Al:=B_Al1+(KK-1)*STEP;
      C_Al:=C_Al1+(LL-1)*STEP;

      if ALLOCATED then
      begin

        {do Xray}
        DeletePowder; {clear out old one }
        SetRadiation(XRAY);
        SetLambda(1.13);
        SetPowderKa2(0,1); {turn off K alpha 2}
        SetPowderRange(10,80,0.05);

        I0_111:=0.0221; I0_002:=0.302; I0_RAT1:=0.0347; I0_RAT2:=0.473; {200C values}

        CALCFIT;
        ERRORX:=ERROR;

        {do neutron}
        DeletePowder; {clear out old one }
        SetRadiation(NEUTRON);
        SetLambda(1.53878);
        SetPowderRange(10,80,0.05);

        I0_111:=0.080; I0_002:=0.023; I0_RAT1:=0.169; I0_RAT2:=0.034; {200C values}

        CALCFIT;
        ERRORN:=ERROR;
        ERROR:=(ERRORX+ERRORN)/2;

        writeln(" E xray :",ERRORX:6:3,"  E neutron :",ERRORN:6:3," E average :",ERROR:7:4);
        if ERROR<OLDERROR then
        begin
          { save this occupancy}
          A_Au_x:=A_Au; A_Al_x:=A_Al;A_Cu_x:=A_Cu;
          B_Au_x:=B_Au; B_Al_x:=B_Al;B_Cu_x:=B_Cu;
          C_Au_x:=C_Au; C_Al_x:=C_Al;C_Cu_x:=C_Cu;
          OLDERROR:=ERROR;
          writeln("error set to ",ERROR:6:4);
        end;

      end; {of if ALLOCATED}
    end; {of II etc loops}

    writeln;
    writeln("Best error avg:",OLDERROR:8:4);
    writeln;

    writeln("     A      B      C");
    writeln("Au ",A_Au_x:5:3,"  ",B_Au_x:5:3,"  ",C_Au_x:5:3);
    writeln("Al ",A_Al_x:5:3,"  ",B_Al_x:5:3,"  ",C_Al_x:5:3);
    writeln("Cu ",A_Cu_x:5:3,"  ",B_Cu_x:5:3,"  ",C_Cu_x:5:3);
    writeln("-----------------------");

    {reset starting guess}
    A_Au1:=A_Au_x;
    B_Au1:=B_Au_x;
    B_Al1:=B_Al_x;
    C_Al1:=C_Al_x;


  until FOREVER;
end;
```

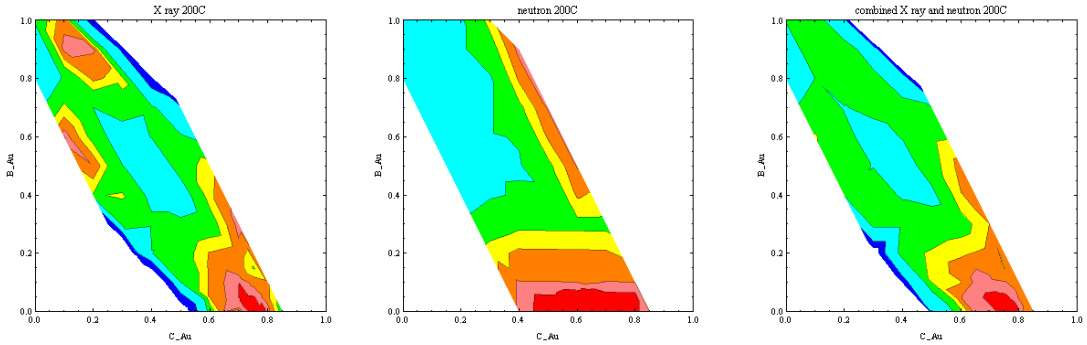

(a) (b) (c)

Fig. S1. Diagrams showing lattice occupancies producing the best fit (red) to data taken at 200ºC. The white regions indicate regions that cannot be occupied in the case of the $Au_7Cu_5Al_4$ stoichiometry. The independent variables were the lattice occupancies of Au. For each of these, the Al occupancies were varied in order to obtain the minimum value of the error, *s*. The contour diagrams show the best value obtained. (a) Possible values of Au on the B and C sites as indicated by the X-ray pattern. (b) Possible values of Au on the B and C sites as indicated by the neutron pattern, (c) Possible values of Au on the B and C sites obtained by combining the X ray and neutron data.

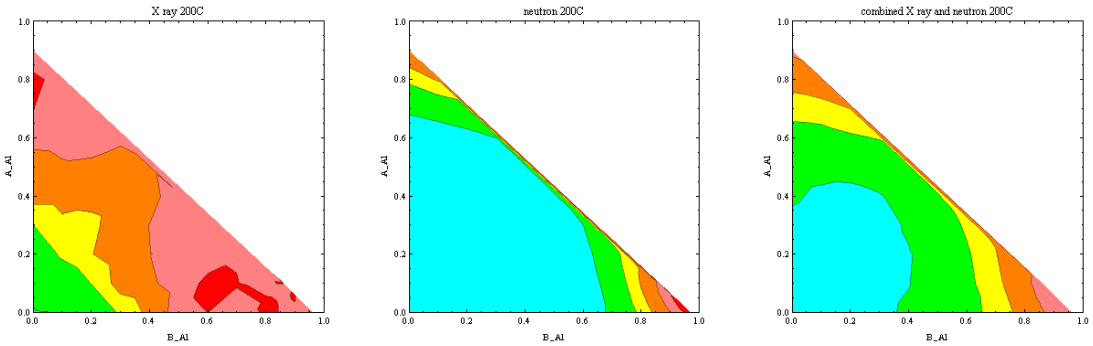

(a) (b) (c)

Fig. S2. Diagrams showing lattice occupancies producing the best fit (red) to data taken at 200ºC. The white regions indicate regions that cannot be occupied in the case of the $Au_7Cu_5Al_4$ stoichiometry. The independent variables were the lattice occupancies of Al. For each of these, the Au occupancies were varied in order to obtain the minimum value of the error, *s*. The contour diagrams show the best value obtained. (a) Possible values of Al on the A and B sites obtained from X-ray data, (b) possible values of Al occupancy obtained from neutron data, (c) Possible values of Al on the A and B sites obtained by combining the X-ray and neutron data.